Spectrochimica Acta Part A: Molecular and Biomolecular Spectroscopy 333 (2025) 125893

Contents lists available at ScienceDirect

Spectrochimica Acta Part A:
Molecular and Biomolecular Spectroscopy

journal homepage: www.journals.elsevier.com/spectrochimica-acta-part-a-molecular-and-biomolecular-spectroscopy

Identification, mapping, and quantification of asbestos minerals in ACM and NOA using NIR-SWIR hyperspectral scan imaging: Preliminary study☆

Lorenzo Marzini [a,*], Iacopo Osticioli [a], Daniele Ciofini [a], Juri Agresti [a], Sergio Bellagamba [b], Federica Paglietti [b], Andrea Azelio Mencaglia [a], Salvatore Siano [a]

[a] Istituto di Fisica Applicata "N. Carrara" – Consiglio Nazionale delle Ricerche (IFAC-CNR), Florence, Italy
[b] Italian Workers Compensation Authority (INAIL), Department of Technological Innovations and Safety of Plants, Products and Anthropic Settlements, Rome, Italy

HIGHLIGHTS

- A novel portable NIR-SWIR hyperspectral point scan imaging tool has been developed.
- NIR reflectance spectra allowed to map and quantify asbestos contents in cement.
- Supercontinuum laser vibrational excitation speeds up NIR-SWIR HSI imaging.

GRAPHICAL ABSTRACT

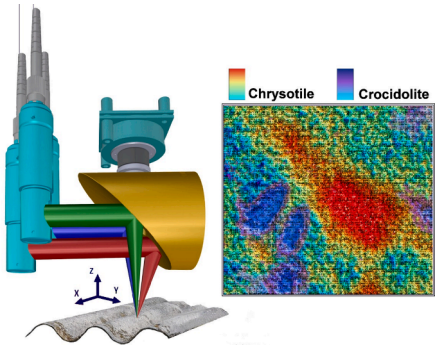

ARTICLE INFO

Keywords:
Asbestos
Hyperspectral imaging
NIR
ACM
NOA
Serpentinites

ABSTRACT

Here, we aimed at extending the Near Infrared-Short-wave infrared (NIR-SWIR) spectroscopy approach in characterizing Asbestos Containing Materials (ACM) and Natural Occurring Asbestos (NOA) through the development and testing of a novel portable asbestos mapping tool based on Hyperspectral Imaging (NIR-HSI) tool. This was built using high resolution spectroscopy over a range of about 170 nm around the OH overtone bands (about 1370–1420 nm), a supercontinuum laser for vibrational excitation, compact XYZ translation stages, and dedicated software. The vibrational reflection data measured using this system allowed discriminating different asbestos minerals and to define the methodological basis for their quantification in various matrices. Point scan NIR-SWIR reflectance images with a spatial resolution of about 50 μm allowed successfully mapping asbestos inclusion in proximity of the surface of a set of samples. The experimentation demonstrated the possibility of characterizing asbestos in NOA or ACM directly *in situ*, through mineral mapping providing qualitative and semi-quantitative information on the asbestos fiber contents.

☆ This article is part of a special issue entitled: 'IASIM-2024 Special Issue' published in Spectrochimica Acta Part A: Molecular and Biomolecular Spectroscopy.

* Corresponding author.
E-mail addresses: L.Marzini@ifac.cnr.it (L. Marzini), I.Osticioli@ifac.cnr.it (I. Osticioli), D.Ciofini@ifac.cnr.it (D. Ciofini), J.Agresti@ifac.cnr.it (J. Agresti), s.bellagamba@inail.it (S. Bellagamba), f.paglietti@inail.it (F. Paglietti), A.mencaglia@ifac.cnr.it (A.A. Mencaglia), S.Siano@ifac.cnr.it (S. Siano).

https://doi.org/10.1016/j.saa.2025.125893
Received 19 September 2024; Received in revised form 2 February 2025; Accepted 10 February 2025
Available online 11 February 2025

1. Introduction

The term "asbestos" refers to a family of phyllosilicate minerals including chrysotile (the fibrous variety of serpentine) and five amphiboles: grunerite (amosite), riebeckite (crocidolite), anthophyllite, tremolite and actinolite [1]. These have been widely used in the past century for thermal insulation, shielding, and sound absorption materials [2,3], as well as in building materials [4], plastic and textile products [5], and other. Such an intensive exploitation of asbestos has been stimulated by its unique physical and chemical, properties. However, Asbestos Containing Materials (ACM) and Naturally Occurring Asbestos (NOA) represent matter of health concerns due to their potential release of fibers because of manipulation and/or alteration. Indeed, biological, physical, and chemical weathering processes can mobilize asbestos fibers from the various matrices, which can hence be dispersed into the environment [6] and produce serious risks for the human health [7–12].

As well known, the inhalation of asbestos fibers represents a serious threat for human health (see for example Hillerdal and Henderson, [13]), thus the introduction of rapid and accurate *in situ* detection and quantification is of primary importance. Indeed, the recognition and quantification of the different fibers is crucial in order to evaluate the specific toxicities, disposal protocols, and possible preventive measures, although such analytical objectives still represent very challenging tasks.

Along the last decades, significant efforts have been dedicated to the characterization of NOA or ACM using laboratory analytical approaches, such as X-ray diffraction (XRD), Fourier transform infrared spectroscopy (FTIR), and scanning electron microscopy (SEM-EDX). Despite these techniques are currently mostly used in asbestos pollution studies, according to a long tradition of works carried out since 1970s [1] and the consequent legal protocols stated by the National governments, they present serious limitations. All the mentioned techniques require sample collection and preparation and their use in quantitative characterizations involve complex and time-consuming analytical protocols. This encourages to spend more efforts in developing efficient portable instruments and associated rapid identification and quantification methods. The potential of *in situ* characterization of ACM or NOA using portable Raman, XRF, and IR spectroscopies has been recently investigated in some works [14–16], which suggest the promising analytical perspectives of vibrational spectroscopy in terms of effectiveness and efficiency, real time detection, cost reduction, and portability. Indeed, the different types of asbestos fibers can be thoroughly discriminated by means of Raman, FTIR, and NIR-SWIR spectroscopies, on the basis of the lattice vibration bands between 1200–500 cm^{-1} [1,17] and a set of spectral features associated with the OH stretching vibrations (3700–3500 cm^{-1}). However, *in situ* application of Raman spectroscopy on ACM is not straightly practicable, while Diffuse Reflectance FTIR has a low spatial resolution then it is not suited for *in situ* imaging applications, which can be conveniently carried out using NIR-SWIR spectroscopy.

Miniaturized NIR-SWIR spectrometers equipped with InGaAs sensor array, which started to be widespread along the last two decades, significantly simplified the development of the corresponding hyperspectral imaging (HSI) systems, which have been then extensively used in remote sensing and proximal imaging in various fields of application. In particular, such an approach has been exploited for mapping the distribution of asbestos over geological areas [18] or urban contexts (asbestos-cement and other ACM) [19]. Furthermore, it has also been extensively used for *in situ* diagnostic applications in biology (see for example Torres Gil et al., [20]) cultural heritage (see for example Picollo et al., [21]), and other by means of experimental setups, which can be adapted to map and evaluate asbestos in ACM and NOA. Recently, NIR-SWIR HSI based on multivariate analysis combined with XRF proved effective for developing a classification method capable of identifying the presence of asbestos fibers in small (~1 cm^2) samples wastes [16].

Here, we aimed at producing a similar mapping of asbestos in different matrices, as that of the latter work, by developing a dedicated portable NIR-SWIR scan tool and a direct mapping of fiber bundles based on standalone spectral features. The system was based on high resolution spectroscopy around the OH overtone bands (about 1370–1420 nm), highly focusable excitation source, compact XYZ translation stages, and dedicated homemade software. The vibrational data measured using the novel system allowed to identify different asbestos minerals in a set of selected samples and to define the conceptual bases for their quantification, thus showing the possibility of characterizing NOA or ACM directly *in situ*, through direct NIR-SWIR mineral mapping.

2. Materials and methods

2.1. ACM and NOA samples

Standards, ACM, and NOA samples analysed in this work are reported in Table 1. ACM and Standard samples were provided by the Italian Workers Compensation Authority (INAIL) Department of Technological Innovations and Safety of Plants, Products and Anthropic Settlements (Rome, Italy) while the NOA sample were provided by the Department of Physical Sciences, Earth and Environment (DSFTA) of University of Siena (Italy). The NOA sample was collected from a serpentinites outcrop located in the Murlo study area (province of Siena, Italy).

Chrysotile ($Mg_3Si_2O_5(OH)_4$) and crocidolite ($Na_2(Mg,Fe)_6Si_8O_{22}(OH)_2$) standard samples were selected (St1, St2) in order to achieve the reference NIR-SWIR spectral datasets.

2.2. Instrumental development

A novel fiber coupled optical probe/head equipped with three confocal channels for intense NIR-SWIR excitation, Vis illumination, and NIR-SWIR reflection collection was designed and built using 3D resin printing, mirrors, and fiber connections, as shown in Fig. 1. The primary focusing and collecting mirror towards the target was a protected silver coating Ø2″ holed 90° off-axis parabolic mirror (Fig. 1a) with a focal length of 2″, and working distance of about 2.5 cm. while fiber couplings were achieved using a secondary Ø½" and 1″ focal length 90° off-axis parabolic mirror for each of the present three optical channels. The hole through the primary mirror was exploited to collect digital images of the area under analysis using a high-definition camera (pixel size of 1.5 μm).

A fiber coupled supercontinuum laser with bandwidth 400–2400 nm and CW power of 100 mW (Samba, LEUKOS, FR) was selected as NIR-SWIR excitation source, while the corresponding reflection channel was fiber coupled to the spectrometer NIRQuest+ (Ocean Optics), which was suitably customized to cover the spectral range 1350–1517 nm with a resolution of about 0.8 nm and then to detect the OH overtone bands with a rather high resolution. Vis illumination by a halogen lamp was also added.

The supercontinuum laser guarantees high spectral power density in

Table 1
List of standards, ACM and NOA selected to perform the HSI based recognition/classification procedures.

ID sample	Sample type	Asbestos species
St1	Standard	Pure chrysotile
St2	Standard	Pure crocidolite
ACM1	Asbesto in organic matrix from a gasket	Chrysotile, crocidolite
ACM2	Asbesto-cement from roof panel	Chrysotile, crocidolite
ACM3	Asbesto-cement from pipe	Chrysotile, crocidolite
NOA	Ranocchiaia (serpentinized peridotite)	Lizardite (serpentine polymorph)

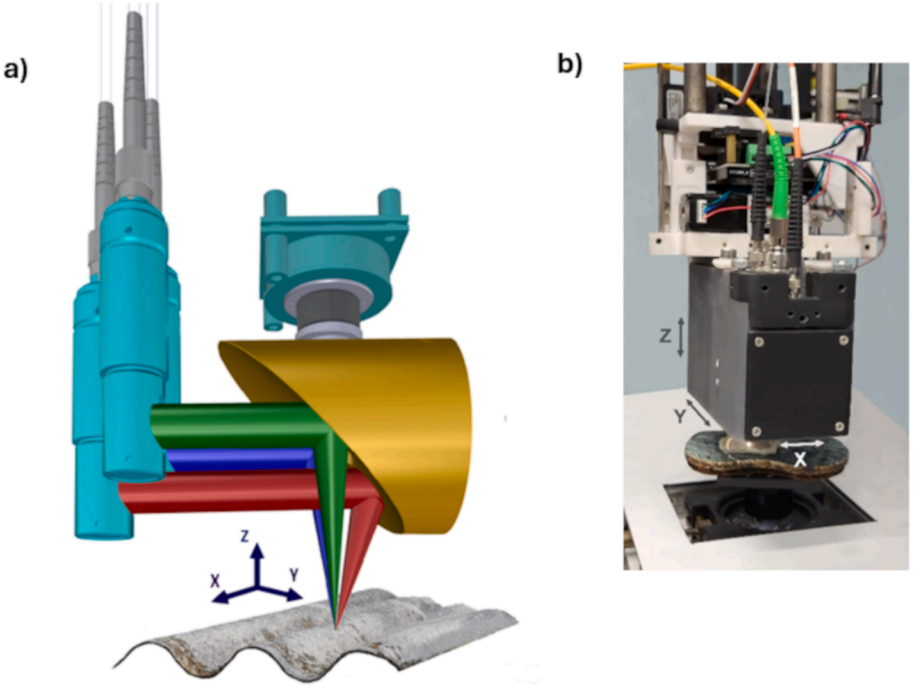

Fig. 1. NIR-SWIR scanning probe: a) optical setup, b) hardware developed.

the region of interest and high focusability, which means intensity over the latter, which is order of magnitude larger than the one provided by a typical focused halogen lamp.

The described optical probe was mounted on a compact XYZ translation group allowing to perform XY scans for collecting reflection maps and implementing the autofocus through the suitable control of the Z axis (see below). Finally, a dedicated software for the overall hardware and acquisition process control, data processing and visualization of the final mineral map was developed (own-built in LabView™ environment). The diameter of the focused NIR-SWIR excitation beam provided by the supercontinuum laser was about 100 μm. However, the actual illumination spot was slightly broadened by scattering and the core diameter of the signal collection fiber was 25 μm, which determined the spatial resolution of the reflection maps, which were collected by scanning areas of ~ 1–100 mm^2. Furthermore, in order to get sufficiently intense reflection signal, at the present stage, spectra were acquired by setting a sampling step of 10 μm and an integration time of about 24 ms. Thus, the overall scanning time and map visualization for a sample surface of about 1 cm^2, corresponding to 1 million spectra, was about 1 h.

2.3. Data processing

To derive the distribution maps of chrysotile and crocidolite in the ACM and NOA samples listed in Tab. 1 the cosine similarity, which is equivalent to the spectral angle mapper (SAM) [22,23] was applied. As well known, the cosine similarity approach is often used to evaluate the similarity between two multidimensional quantities such as, in particular, two spectra represented by the respective vectors corresponding to their respective cartesian ordinates. It is defined as the cosine of the plane angle between the actual spectrum vector and that of a known material assumed as reference, which range between −1 (antiparallel = not similar) and 1 (parallel = maximum similarity).

Here, the cosine metrics was applied to automatically discriminate chrysotile or crocidolite in ACM and NOA through the comparison with the respective standards. Thus, the XY mapping of such a parameterization selectively reproduced the distribution of the mentioned asbestos minerals, which was achieved by means of a homemade LabVIEW™ code.

The NIR-SWIR scan images of NOA and ACM samples, achieved as described above, were processed through the application of unsupervised classification clustering algorithm based on the Iterative Self-Organizing Data Analysis (ISODATA) technique [24,25]. This data processing algorithm allows the automatic adjustment of the number of image clusters during the iteration by merging similar clusters and splitting clusters with large standard deviations. It uses a maximum-likelihood decision rule to calculate class averages that are uniformly distributed in the space and then iteratively clusters the remaining pixels using minimum-distance criterion so that a cluster represents groups of pixels within a multivariate space [26,27]. The performances of the selected classification method were evaluated and compared in terms of classified images. Statistical and classification analyses were performed using ArcMAP software (ESRI™).

3. Results

The novel NIR-SWIR point scan hyperspectral imaging system, its instrumental control software, and associated image processing to extract asbestos distribution maps, which were developed in the present work, were formerly thoroughly tested and underwent several improvement phases. In particular, the significant spectral fluctuation of the supercontinuum laser output required a suitable combined selection of the spectral interval parameterized by means of the cosine metrics, integration time (set at between 10–20 ms), and core diameter of the signal collection fiber (∅25 μm was selected). Furthermore, after testing several potential solutions for the autofocus mechanism the actual solution was achieved by exploiting the non-perfect orthogonality between the optical axis and the sample surface, which produced a slight micro-shift of the Vis spot provided by the halogen lamp when moving the probe along the Z axis. Thus, the autofocus routine was built based on the continuous recovery of the XY position of the spot barycentre at the focal plane.

Fig. 2 shows the characteristic OH overtone bands of chrysotile and crocidolite at 1380 nm and 1415 nm [16,28,29]), respectively, as measured using the present setup (Fig. 1) with halogen lamp (Fig. 2a-c) or supercontinuum laser (Fig. 2b-d) excitation, respectively. As shown,

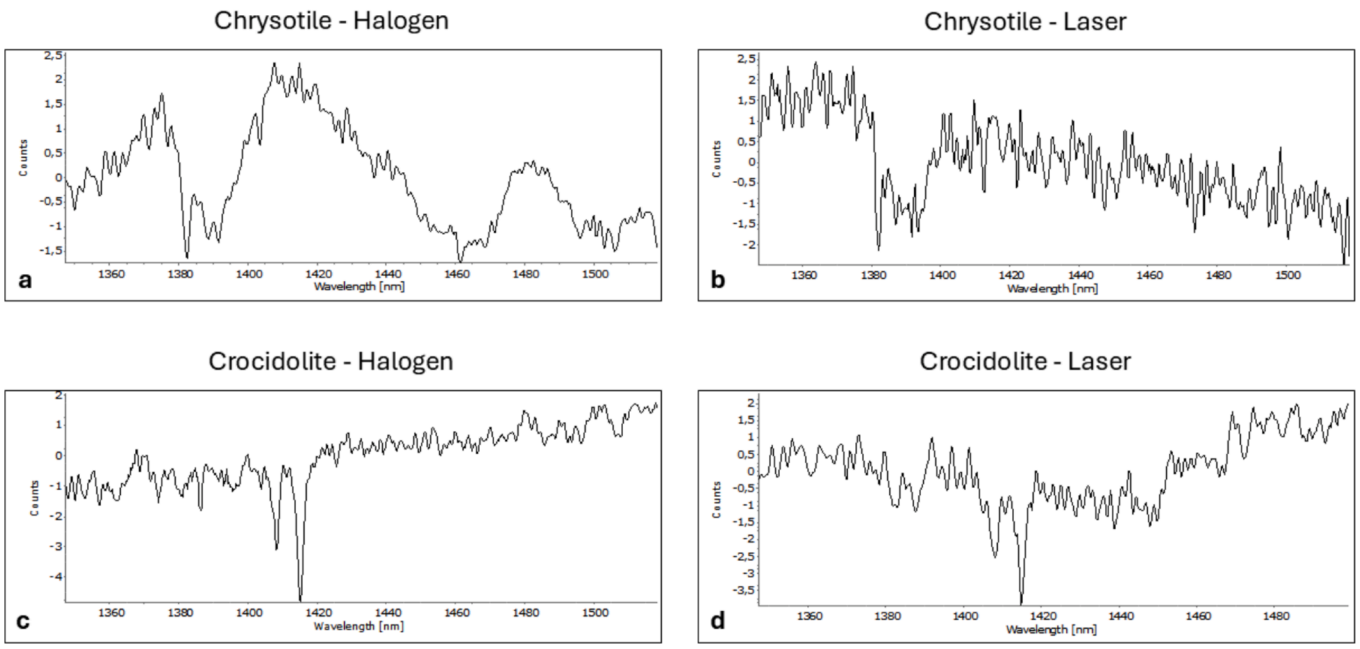

Fig. 2. NIR-SWIR spectra (after Standard Normal Variates-SNV operation) of chrysotile (a-b) and crocidolite (c-d) as collected under halogen lamp (a, c) and laser (b, d) excitation using acquisition times of 5 s and 20 ms, respectively.

the higher spectral power density of the latter allowed a significant reduction of the acquisition times (20 ms against 5 s), which made feasible the present mineral scan mapping approach.

The mentioned overtone bands, which allow discriminating chrysotile and crocidolite thanks to the energy differences between the OH vibrational levels within the two corresponding crystal structures, were assumed as references for the cosine metrics used for processing hyperspectral scan images and transform them in mineral maps.

Examples of ACM mineral map layers of chrysotile and crocidolite, respectively, over an almost square area of about 3 mm^2 are displayed in Fig. 3b–c, which refers to the sample ACM3 listed in Table 1. Fig. 3a displays the Vis image of the area analysed as captured by the video camera. The examination of the Vis image is obviously also important for assessing the petrographic coherence.

Fig. 4 shows the output maps after the application of the ISODATA algorithm (unsupervised classification) with the detection of crocidolite and chrysotile red spots are reported, which provide a simple way to calculate the areal fraction of the asbestos minerals. In general, such a datum will get meaningful when extracted from one or several measurements over a representative total area, which in principle must be much larger than the sizes of the asbestos inclusions.

Selective mineral map of ACM2 over about 3 × 3 mm^2 area is reported in Fig. 5, while the corresponding processed maps following the application of the ISODATA algorithm (unsupervised classification), highlighting crocidolite and chrysotile micro domains (red spots) are displayed in Fig. 6.

Asbesto mineral maps over an area of 100 mm^2 (1 million acquisitions) of ACM1 and the corresponding ISODATA output are shown in Fig. 7, where only chrysotile spots (red colour in Fig. 7c) are present.

Finally, the scan results of NOA1 sample over about 100 mm^2 area are reported in Fig. 8. Vis examination of this sample showed the typical features of such a ultramafic rock, which is characterized by a dense distribution of locally oriented dark veins and veinlets within the serpentine that appears as an agglomerate of granular white-greenish patches. As known the former petrographic feature is attributable to magnetite distribution while the latter corresponds to lizardite, a serpentine polymorph with OH stretching spectral signature coincident with that of chrysotile. The measured maps reflect this petrographic

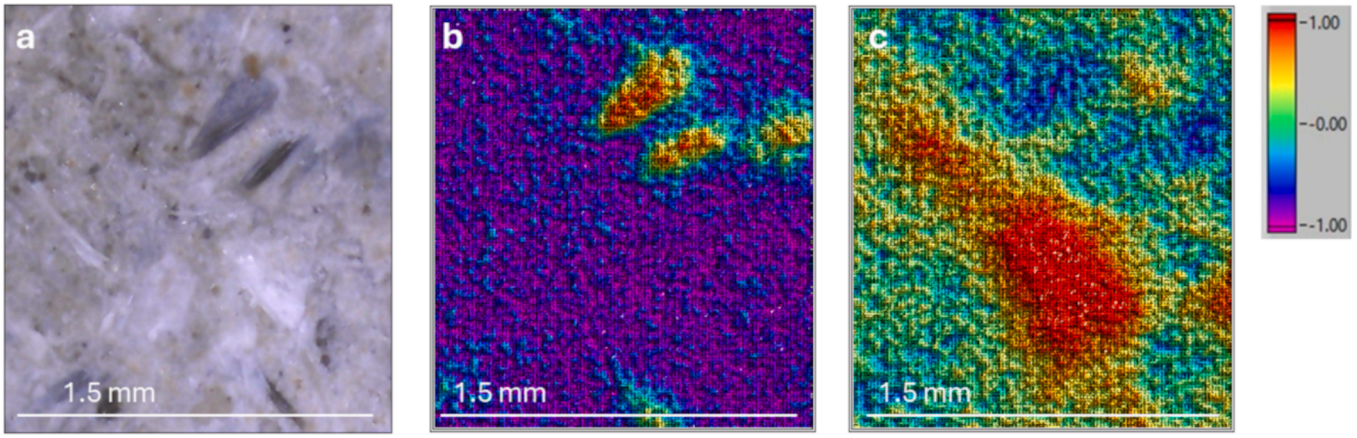

Fig. 3. Example of NIR-SWIR mineral mapping of chrysotile and crocidolite over about 3 mm^2 area of the sample ACM3: a) Vis image (see the text), b) distribution map of crocidolite, c) distribution map of chrysotile (deep red colour corresponds to maximum similarity, violet colour to absence of similarity).

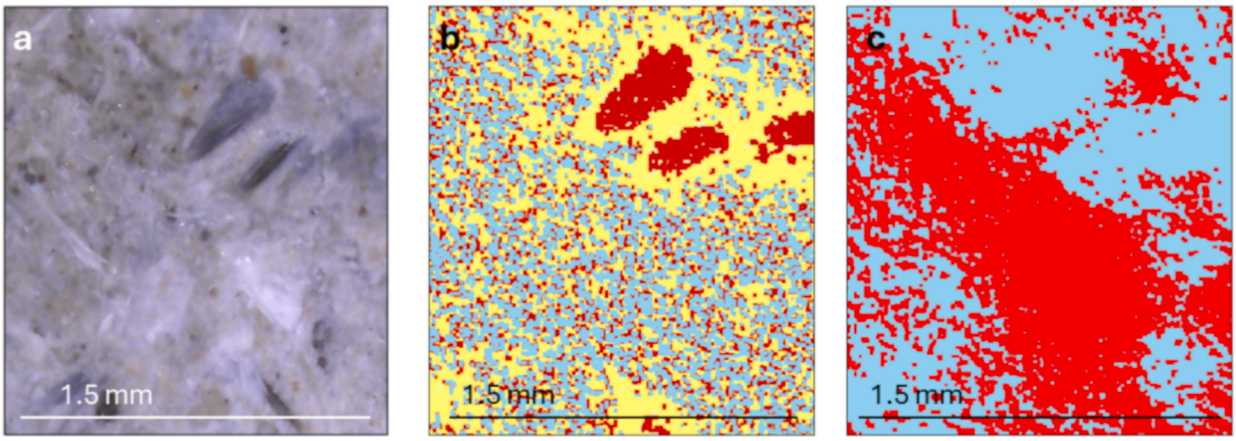

Fig. 4. Results of the unsupervised classification analysis related of the sample ACM3: a) Vis image of area under analysis, b) classification map of crocidolite (red spots), classification map related to chrysotile (red spots).

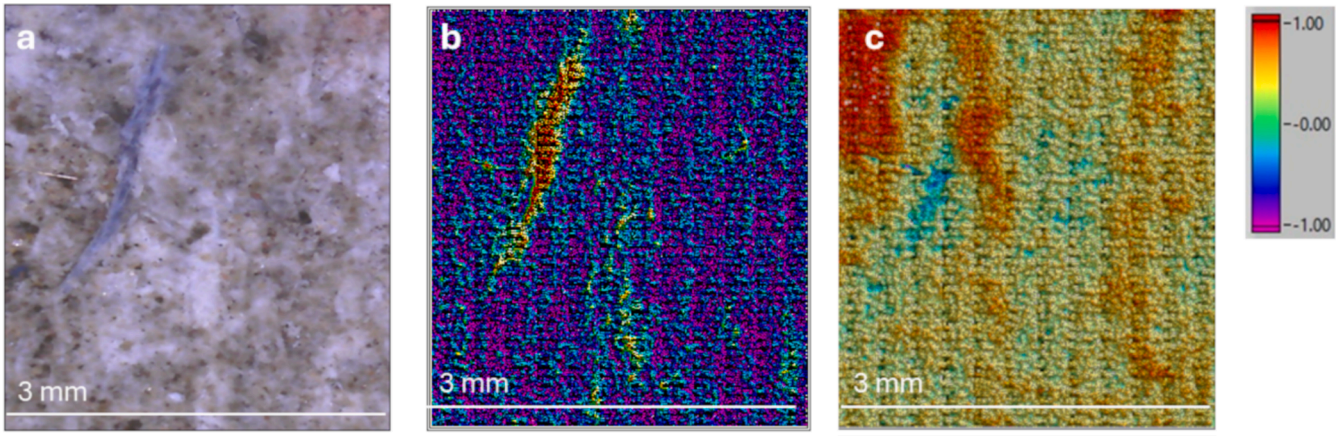

Fig. 5. NIR-SWIR selective mapping of asbestos components of the sample ACM2: a) Vis image, b) map of crocidolite, c) map of chrysotile.

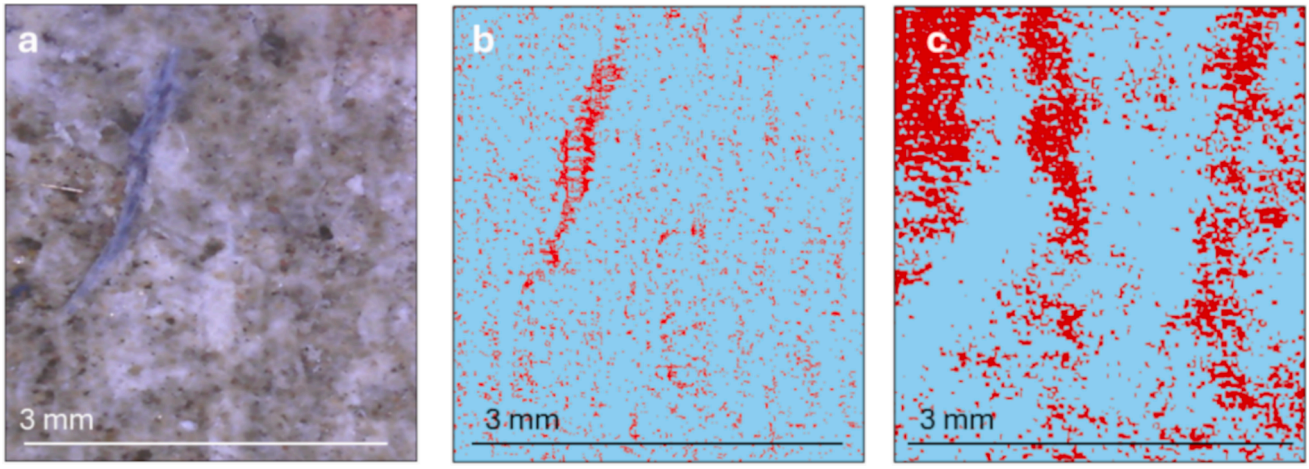

Fig. 6. Unsupervised classification analysis of the sample ACM2 corresponding to the data sets of Fig. 5: a) Vis image, b) crocidolite, c) chrysotile.

interpretation, as shown in Fig. 8, where colours similar to the real ones were used for improving the comparison of the final mineral map with the Vis image.

4. Discussion

The danger of asbestos fibers for human health stimulated a large number of material characterization studies involving different spatial scales, which range from that of geological and urban survey to that of nano-structural analysis using a broad set of analytical techniques. In all the cases the characterization at the microscopic and mesoscopic scales, along with the quantification of the fibers within a given material are crucial for assessing the potential pathogenicity hazards. Compositional and crystallographic analyses at the microscopic and mesoscopic scales

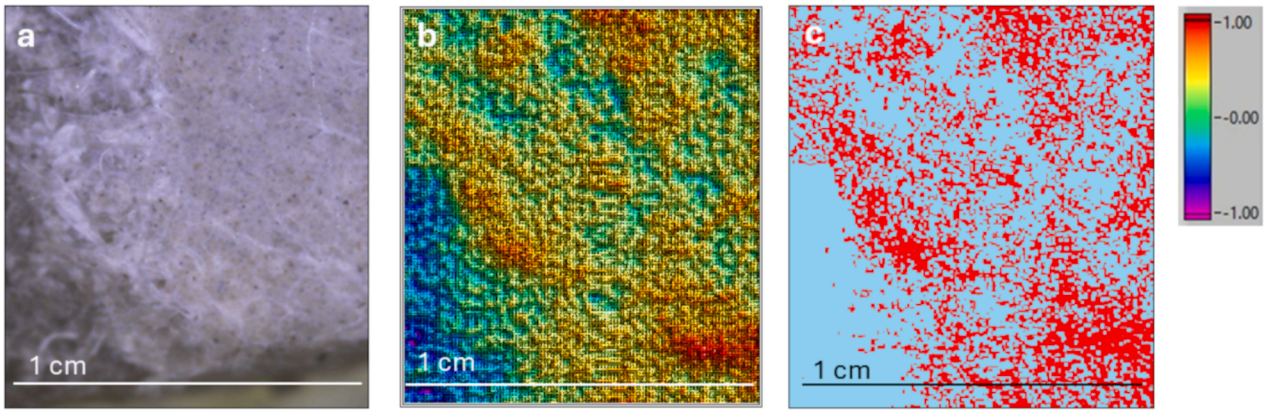

Fig. 7. ACM1 scan: a) Vis image, b) chrysotile mineral map, c) unsupervised classification.

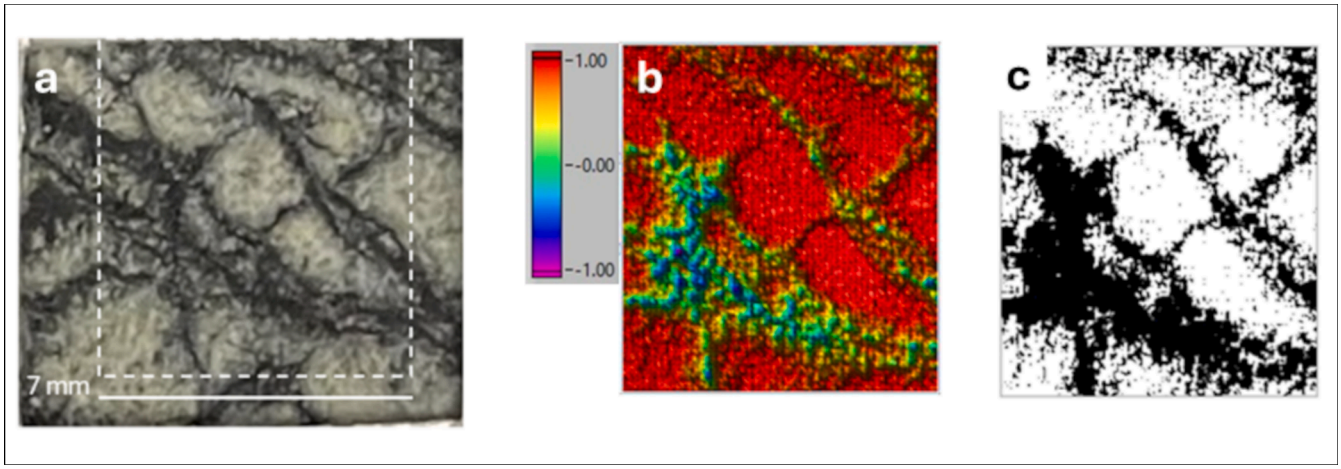

Fig. 8. Sample NOA1 (Ranocchiaia): a) Vis. Image (study area highlighted by the white dashed square), b) lizardite map as derived using the cosine similarity, c) lizardite map after the unsupervised classification processing.

are relatively complex since they involve the so-called matrix effects and the need of high resolution, which can be approached through sample manipulations and laboratory instrumentations. To overcome the risks of fiber releases along with cost and time-consuming problems associated to the latter we developed and successfully tested a portable NIR-SWIR HSI tool for identifying and evaluating the asbestos in a given sample in any context and without any preliminary preparation. The results presented above show its effectiveness in collecting hyperspectral scan images, which were used to selectively extract chrysotile and crocidolite maps, respectively, reflecting mostly their distributions over the scanned surface.

It is important to point out that despite the presence of several minerals, the present analysis was very selective, and the heterogeneity of the ACM investigated did not affect the mapping. This was essentially determined by absence of spectral superpositions at the high spectral resolution of the system developed. This was obvious for ACM1 and NOA1, whereas asbestos cement of ACM2 and ACM3 could include OH overtone spectral components due to hydrate calcium silicates, typically formed in cement, and gypsum, which is usually added in small amounts. Fortunately, thanks to the present spectral resolution (about 0.8 nm), in both cases the corresponding band peaks are sufficiently far from the ones of chrysotile and crocidolite, respectively, and then they were cut out from the elaboration spectral intervals selected. In particular, the bands of hydrate calcium silicates are centered around 1410 nm (see for example Pineau et al., [30]), those of gypsum around 1445 nm (see for example Camaiti et al., [31]), and the elaboration ranges for chrysotile and crocidolite were set between 1378–1382 and 1414–1418 nm, respectively.

A further important aspect to be discussed concerns the spatial resolution, which is determined here by the core diameter of the collection fiber. According to the sensitivity of the present setup, ∅50 μm was selected with the perspective of reducing it at ∅25 μm or less after some further improvements to be carried out on the system.

The resolution of 50 μm can allowed resolving asbestos fragments and fiber bundles separated by a larger distance, which allow achieving reconstructing mineral mappings such as as those showed in Figs. 3, 5, 7, which correspond to a first level of accuracy. Nevertheless, these hyperspectral scanning results represent a good starting point for qualitative and semi-quantitative evaluations of the asbestos fiber contents in ACM. For example, the presence of chrysotile fibers or bundles in ACM3 (Fig. 3b–c), which were not distinguishable in the Vis image (Fig. 3a), were promptly identified and mapped (Fig. 4b–c). Similarly, both evident and not evident bluish fibers of crocidolite were spectrally recognised, mapped (Fig. 5a–b, Fig. 6a–b), and eventually quantitatively evaluated. For example, the present approach applied to the sample ACM2 returned chrysotile and crocidolite contents of 13 % and 12 % average areal fractions, respectively, as calculated by averaging the results of HSI over 8 different areas of the sample of about 50 mm^2 each. This result is apparently congruent with the typical composition of the asbestos cement, although accurate quantifications certainly require further investigations.

The measurements carried out on the sample NOA1 (Fig. 8) provided a good demonstration of the reliability of the present compositional mapping but, at the same time, they also confirmed that standalone OH

overtone bands do not allow to discriminate the polymorphs of the serpentine group (antigorite, chrysotile, lizardite). The latter are phyllosilicates with the same composition ($Mg_3Si_2O_5(OH)_4$ and basic structure given by a repeated two-layer arrangement with one tetrahedral (SiO_4) and one octahedral ($Mg(OH)_2$) layer, respectively [32]. The crystallographic differences among the polymorphs are represented by deformation and disposition of the mentioned two-layer structure [32,33]. The measurement carried out on NOA1 showed such structural differences did not induce any significant difference of the OH overtone vibration bands of lizardite with respect to those of chrysotile, in agreement with the literature [33,34]. The investigation on the possible discrimination of the polymorphs should hence be extended over a larger spectral range, which will be subject of forthcoming studies.

Conversely, the results achieved in this study prove NIR-SWIR HSI is very effective in ACM characterization, which can safely be achieved without preliminary manipulation of the sample thus preventing risks of inhalation of asbestos fibers. Indeed, in the perspective of hazard evaluation, it is fundamental to rapidly recognize and quantify the amount of fibrous minerals in a variety of ACM. To date, a few studies described a methodology able to distinguish the asbestos minerals directly *in situ* on the sample as it is [1,35], without removing the fibers from the matrix, and no one reported *in situ* quantification methodologies.

Here, chrysotile and crocidolite asbestos were considered for the NIR-SWIR HSI analysis since these asbestos minerals have been the most used in in ACM produced in Italy [36]. The extension of the data processing to amosite and the other amphiboles will further improve the present methodology, which offers a smart and affordable solution for the analytical support in asbestos remediation activities, while the possible solution of the discrimination problem of polymorphs could make standalone portable NIR-SWIR HSI a powerful analytical approach and allow its applicative extension to building yards and mining.

5. Conclusions

In the present work, a compact portable NIR-SWIR HSI system and a methodology to exploit it in recognition, mapping, and quantification of chrysotile and crocidolite in ACM were developed and successfully demonstrated trough a set of measurements carried out on samples of interest. Such a chemical sensor allowed performing rapid compositional mapping of ACM and NOA, although in the latter case a reliable solution for discriminating the polymorphs of serpentine is still under study. The novel system allowed collecting and processing 1 million spectra/hour and produced maps of the asbestos minerals without any preliminary treatment of the sample, with a resolution of 50 μm. Data were processed through an unsupervised classification analysis based on the comparison of the collected spectra with those of pure chrysotile and crocidolite., by means of a dedicated software protocol.

The methodology described is very promising for rapid assessments in several operative contexts. It could allow overcoming time, costs, and representativeness issues of the traditional characterization based on laboratory equipment such as SEM, FTIR, XRD and related sample preparation phases.

Further insights will be dedicated to the refinement of the technology and method presented in this work and the extension of the discrimination and classification processing to the polymorphs of serpentine by investigating a spectral range broader than the present one and, besides crocidolite, to other amphibole asbestos minerals.

6. Data statement

All data generated or analysed for this study are included in this article, and the related datasets are available from the corresponding author upon reasonable request.

7. Funding sources

This work was carried out within the project SIC-QUAM "*Development of an imaging system for in situ identification and quantification of asbestos fibers in ACM*" co-funded by Italian Workers Compensation Authority (INAIL, Bric 2022, ID 70).

CRediT authorship contribution statement

Lorenzo Marzini: Formal analysis, Investigation, Visualization, Writing – original draft. **Iacopo Osticioli:** Funding acquisition, Investigation. **Daniele Ciofini:** Methodology, Investigation. **Juri Agresti:** Investigation. **Sergio Bellagamba:** Supervision. **Federica Paglietti:** Funding acquisition, Validation. **Andrea Azelio Mencaglia:** Formal analysis, Methodology, Software, Visualization. **Salvatore Siano:** Conceptualization, Writing – review & editing, Resources, Supervision.

Declaration of competing interest

The authors declare that they have no known competing financial interests or personal relationships that could have appeared to influence the work reported in this paper.

Acknowledgements

The present work was carried out within the activities of the project SIC-QUAM "Development of chemical imaging instrumentation for the identification and in situ quantitative evaluation of asbestos fiber content in ACM" co-funded by INAIL (BRIC 2022, ID 70) and CNR. Authors wish also to thank Prof. Cecilia Viti of the University of Siena for providing the NOA sample investigated in this work and related informations.

Data availability

Data will be made available on request.

References

[1] V. Zholobenko, F. Rutten, A. Zholobenko, A. Holmes, In situ spectroscopic identification of the six types of asbestos, J. Hazard. Mater. 5 (403) (2021 Feb) 123951, https://doi.org/10.1016/j.jhazmat.2020.123951.

[2] G.M. Militello, L. Gaggero, S. La Maestra, Asbestiform Amphiboles and Cleavage Fragments Analogues: Overview of Critical Dimensions, Aspect Ratios, Exposure and Health Effects, Minerals. 11 (5) (2021) 525, https://doi.org/10.3390/min11050525.

[3] S. Bolan, L. Kempton, T. McCarthy, H. Wijesekara, U. Piyathilake, T. Jasemizad, L. P. Padhye, T. Zhang, J. Rinklebe, H. Wang, M.B. Kirkham, K.H.M. Siddique, N. Bolan, Sustainable management of hazardous asbestos-containing materials: Containment, stabilization and inertization, Sci. Total Environ. 881 (2023), https://doi.org/10.1016/j.scitotenv.2023.163456. ISSN 0048-9697.

[4] F. Vergani, L. Galimberti, N.M. Marian, G. Giorgetti, C. Viti, G.C. Capitani, et al., Thermal decomposition of cement–asbestos at 1100 °C: how much "safe" is "safe"? J. Mater. Cycles Waste Manage. 24 (2022) 297–310, https://doi.org/10.1007/s10163-021-01320-6.

[5] R.L. Virta, Asbestos: Geology, Mineralogy, Mining, and Uses, U.S. Department of the Interior, U.S. Geol. Surv. Open File Rep. (2002) 02–149.

[6] T. Ervik, E. Hammer, P. Graff, Mobilization of asbestos fibers by weathering of a corrugated asbestos cement roof, J. Occup. Environ. Hyg. 18 (3) (2021 Mar) 110–117, https://doi.org/10.1080/15459624.2020.1867730.

[7] R.J. Lee, B.R. Strohmeier, K.L. Bunker, D.R. Van Orden, Naturally occurring asbestos: a recurring public policy challenge, J. Hazard. Mater. 153 (1–2) (2008 May 1) 1–21, https://doi.org/10.1016/j.jhazmat.2007.11.079.

[8] F. Giacomini, V. Boerio, S. Polattini, M. Tiepolo, R. Tribuzio, A. Zanetti, Evaluating asbestos fibre concentration in metaophiolites: a case study from the Voltri Massif and Sestri-Voltaggio Zone (Liguria, NW Italy) Environ, Earth Sci. 61 (2010) 1621–1639.

[9] L. Gaggero, L. Crispini, E. Isola, P. Marescotti. Asbestos in natural and anthropic ophiolitic environments: a case study of geohazards related to the northern apennine ophiolites (Eastern Liguria, Italy) Ofioliti, 31 (1) (2013), pp. 29-40.

[10] G. Belardi, G. Vignaroli, F. Trapasso, A. Pacella, D. Passeri, Detecting asbestos fibres and cleavage fragments produced after mechanical tests on ophiolite rocks: clues for the asbestos hazard evaluation, J. Mediterranean Earth Sci. X (2018), https://doi.org/10.3304/JMES.2018.016.

[11] R. Cossio, C. Albonico, A. Zanella, S. Fraterrigo-Garofalo, C. Avataneo, R. Compagnoni, F. Turci, Innovative unattended SEM-EDS analysis for asbestos fiber quantification, Talanta 190 (2018) 158–166, https://doi.org/10.1016/j.talanta.2018.07.083. ISSN 0039-9140.
[12] L. Marzini, M. Iannini, G. Giorgetti, F. Bonciani, P. Conti, R. Salvini, C. Viti, Asbestos Hazard in Serpentinite Rocks: Influence of Mineralogical and Structural Characteristics on Fiber Potential Release, Geosciences 14 (8) (2024) 210, https://doi.org/10.3390/geosciences14080210.
[13] G. Hillerdal, D.W. Henderson, Asbestos, asbestosis, pleural plaques and lung cancer, Scand. J. Work Environ. Health 23 (2) (1997) 93–103.
[14] A. Croce, D. Bellis, C. Rinaudo, L. Cagna, G. Gatti, A. Roveta, M. Bertolotti, A. Maconi, Application of a Multi-Technique Approach to the Identification of Mineral Polymorphs in Histological Samples: A Case of Combined Use of SEM/EDS and Micro-Raman Spectroscopy, Minerals. 14 (7) (2024) 633.
[15] J.R. Petriglieri, E. Salvioli-Mariani, L. Mantovani, M. Tribaudino, P.P. Lottici, C. Laporte-Magoni, D. Bersani, Micro-Raman mapping of the polymorphs of serpentine, J. Raman Spectrosc. 46 (2015) 953–958, https://doi.org/10.1002/jrs.4695.
[16] G. Bonifazi, G. Capobianco, S. Serranti, O. Trotta, S. Bellagamba, S. Malinconico, F. Paglietti, Asbestos detection in construction and demolition waste by different classification methods applied to short-wave infrared hyperspectral images, Spectrochim. Acta A Mol. Biomol. Spectrosc. 307 (2024) 123672, https://doi.org/10.1016/j.saa.2023.123672.
[17] G. Della Ventura, R. Vigliaturo, R. Gieré, S. Pollastri, A.F. Gualtieri, G. Iezzi, InfraRed Spectroscopy of the Regulated Asbestos Amphiboles, Minerals. 8 (9) (2018) 413, https://doi.org/10.3390/min8090413.
[18] H. Kumar, A.S. Rajawat, Aqueous alteration mapping in Rishabdev ultramafic complex using imaging spectroscopy, Int. J. Appl. Earth Observ. Geoinform. 88 (2020), https://doi.org/10.1016/j.jag.2020.102084. ISSN 1569-8432.
[19] M. Sabat, N. Fares, G. Mitri, A. Kfoury, Determination of asbestos cement rooftop surface composition using regression analysis and hyper-spectral reflectance data in the visible and near-infrared ranges, J. Hazardous Mater. 469 (2024), https://doi.org/10.1016/j.jhazmat.2024.134006. ISSN 0304-3894.
[20] I. Torres, M.T. Sánchez, B.K. Cho, A. Garrido-Varo D. Pérez-Marín "Setting up a methodology to distinguish between green oranges and leaves using hyperspectral imaging", Proc. SPIE 11421, Sensing for Agriculture and Food Quality and Safety XII, 114210X (22 April 2020); Doi: 10.1117/12.2559102.
[21] M. Picollo, C. Cucci, A. Casini, L. Stefani, Hyper-Spectral Imaging Technique in the Cultural Heritage Field: New Possible Scenarios, Sensors 20 (10) (2020) 2843, https://doi.org/10.3390/s20102843.
[22] R.H.Yuhas,A.F.H Goetz,J.W. Boardman, 1992. Discrimination among semi-arid, landscape endmembers using spectral angle mapper (SAM) algorithm. Summaries of, the 4th Annual JPL Airborne Geoscience Workshop, JPL Pub-92-14, AVIRIS, Workshop. Jet. Propuls. Lab., Pasadena, CA 147–150.
[23] L. Ramirez-Lopez, T. Behrens, K. Schmidt, R.A. Viscarra Rossel, J.A.M. Demattê, T. Scholten, Distance and similarity-search metrics for use with soil vis–NIR spectra, Geoderma 199 (2013) 43–53, https://doi.org/10.1016/j.geoderma.2012.08.035. ISSN 0016-7061.
[24] J.T. Tou, R.C. Gonzalez, Pattern Recognition Principles, Addison-Wesley Publishing, Boston MA, USA, 1974.
[25] A.M. Melesse, J.D. Jordan, A comparison of fuzzy vs. augmented-ISODATA classification algorithms for cloud-shadow discrimination from Landsat images, Photogramm. Eng. Remote Sens. 68 (2002) 905–912.
[26] B.J. Irvin, S.J. Ventura, B.K. Slater, Fuzzy and isodata classification of landform elements from digital terrain data in Pleasant Valley, Wisconsin, Geoderma 77 (2–4) (1997) 137–154, https://doi.org/10.1016/S0016-7061(97)00019-0. ISSN 0016-7061.
[27] L. Marzini, E. D'Addario, M.P. Papasidero, F. Chianucci, L. Disperati, Influence of Root Reinforcement on Shallow Landslide Distribution: A Case Study in Garfagnana (Northern Tuscany, Italy), Geosciences 13 (11) (2023) 326, https://doi.org/10.3390/geosciences13110326.
[28] E. Balan, E. Fritsch, G. Radtke, L. Paulatto, F. Juillot, F. Baron, S. Petit, First-principles modeling of the infrared spectrum of Fe- and Al-bearing lizardite, Eur. J. Mineral. 33 (2021) 647–657, https://doi.org/10.5194/ejm-33-647-2021.
[29] C. Laukamp, K.A. Termin, B. Pejcic, M. Haest, T. Cudahy, Vibrational spectroscopy of calcic amphiboles-applications for exploration and mining, Eur. J. Mineral. 24 (5) (2012) 863–878.
[30] M. Pineau, L. Le Deit, B. Chauviré, J. Carter, B. Rondeau, N. Mangold, Toward the geological significance of hydrated silica detected by near infrared spectroscopy on Mars based on terrestrial reference samples, Icarus 347 (2020), https://doi.org/10.1016/j.icarus.2020.113706. ISSN 0019-1035.
[31] M. Camaiti, S. Vettori, M. Benvenuti, L. Chiarantini, P. Costagliola, F. Di Benedetto, S. Moretti, F. Paba, E. Pecchioni, Hyperspectral sensor for gypsum detection on monumental buildings, J. Geophys. Eng. 8 (3) (2011) S126–S131, https://doi.org/10.1088/1742-2132/8/3/S12.
[32] R. Demichelis, M. De La Pierre, M. Mookherjee, C.M. Zicovich-Wilson, R. Orlando, Serpentine polymorphism: A quantitative insight from first-principles calculations, CrstEngComm 18 (2016) 4412–4419.
[33] E. Fritsch, E. Balan, S. Petit, F. Juillot, Structural, textural, and chemical controls on the OH stretching vibrations in serpentine-group minerals, Eur. J. Mineral. 33 (2021) 447–462, https://doi.org/10.5194/ejm-33-447-2021.
[34] E. Balan, A.M. Saitta, F. Mauri, C. Lemaire, F. Guyot, First-principles calculation of the infrared spectrum of lizardite, Am. Mineral. 87 (2002) 1286–1290, https://doi.org/10.2138/am-2002-1003.
[35] J.R. Petriglieri, L. Barale, C. Viti, P. Ballirano, E. Belluso, M.R. Bruno, A. Campopiano, A. Cannizzaro, M. Fantauzzi, F. Gianchiglia, M.R. Montereali, E. Nardi, A. Olori, F. Piana, M. Tomatis, A. Rossi, H. Skogby, A. Pacella, F. Turci, From field analysis to nanostructural investigation: A multidisciplinary approach to describe natural occurrence of asbestos in view of hazard assessment, J. Hazardous Mater. 457 (2023) 131754, https://doi.org/10.1016/j.jhazmat.2023.131754.
[36] A. Campopiano, A. Cannizzaro, A. Olori, F. Angelosanto, D. Ramires, F. Basili, G. Gargaro, S. Massera, G. Novembre, F. Cavariani, F. Brizi, M. Di Francesco, G. Castri, A. Chiodo, B. Bruni, S. Iavicoli, Asbestos containing materials in schools of Rome and surrounding area (Italy), Ind. Health 59 (6) (2021 Nov 29) 436–448, https://doi.org/10.2486/indhealth.2021-0036.